01 Jan 2022

Regulation of Dendrite-Free Li Plating Via Lithiophilic Sites on Lithium-Alloy Surface

Yufang He

Mengyun Zhang

Aiping Wang

Bo Zhang

et. al. For a complete list of authors, see https://scholarsmine.mst.edu/mec_aereng_facwork/4961

Recommended Citation

Y. He and M. Zhang and A. Wang and B. Zhang and H. Pham and Q. Hu and L. Sheng and H. Xu and L. Wang and J. Park and X. He, "Regulation of Dendrite-Free Li Plating Via Lithiophilic Sites on Lithium-Alloy Surface," *ACS Applied Materials and Interfaces*, American Chemical Society, Jan 2022.
The definitive version is available at https://doi.org/10.1021/acsami.2c05801

ACS APPLIED MATERIALS & INTERFACES

www.acsami.org

Research Article

Regulation of Dendrite-Free Li Plating via Lithiophilic Sites on Lithium-Alloy Surface

Yufang He, Mengyun Zhang, Aiping Wang, Bo Zhang, Hiep Pham, Qiao Hu, Li Sheng, Hong Xu, Li Wang,* Jonghyun Park,* and Xiangming He*

Cite This: *ACS Appl. Mater. Interfaces* 2022, 14, 33952–33959

Read Online

ACCESS | Metrics & More | Article Recommendations | Supporting Information

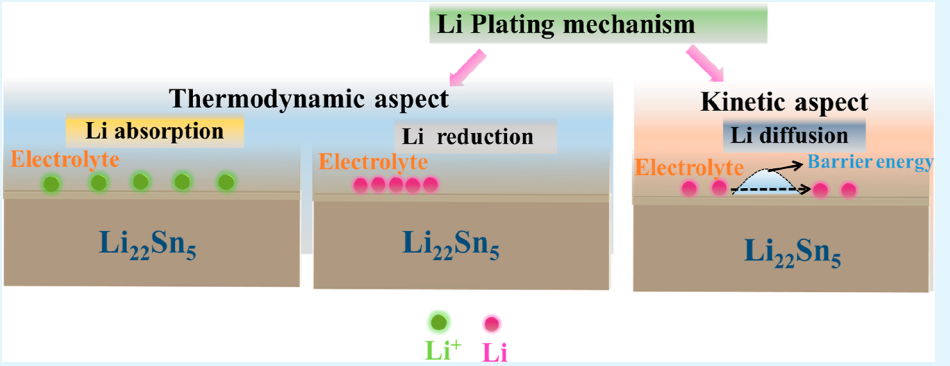

ABSTRACT: Lithium (Li) deposition behavior plays an important role in dendrite formation and the subsequent performance of lithium metal batteries. This work reveals the impact of the lithiophilic sites of lithium-alloy on the Li plating process via the first-principles calculations. We find that the Li deposition mechanisms on the Li metal and $Li_{22}Sn_5$ surface are different due to the lithiophilic sites. We first propose that Li plating on the Li metal surface goes through the "adsorption−reduction−desorption−heterogeneous nucleation−cluster drop" process, while it undergoes the "adsorption−reduction−growth" process on the $Li_{22}Sn_5$ surface. The lower adsorption energy contributes to the easy adsorption of Li on the lithiophilic sites of the $Li_{22}Sn_5$ surface. The lower Li reduction energy on the Li metal surface indicates that it is easy for Li to be reduced on the Li metal surface, attributed to its higher Fermi energy level. Furthermore, the faster Li diffusion on the $Li_{22}Sn_5$ surface results in smooth Li deposition, which is based on a "two-Li synergy diffusion" mechanism. However, Li diffuses more slowly on the Li metal surface than on the $Li_{22}Sn_5$ surface due to the "single Li diffusion" mechanism. This work provides a fundamental understanding on the impact of lithiophilic sites of Li alloy on the Li plating process and points out that the future design of 3D Li-alloy substrates decorated with multilithiophilic sites can prevent dendrite formation on the lithium-alloy substrate by guiding uniform Li deposition.

KEYWORDS: *the first-principles, adsorption energy, reduction energy, lithiophilic sites, Li diffusion*

INTRODUCTION

Lithium-ion batteries (LIBs)[1−4] are omnipresent in daily life and are critical for numerous applications including portable electronics, electric vehicles, and the power grid. However, the traditional graphite anode-based LIBs have limited energy density that cannot meet the increasing market demands for a longer cycle life.[5] Compared with the conventional graphite anode, lithium (Li) metal is regarded as the most promising anode material for next-generation rechargeable batteries owing to its high theoretical capacity (3860 mA h/g) and low chemical potential (−3.04 V vs standard hydrogen electrode).[6,7] However, lithium metal batteries (LMBs) suffer from undesirable SEI layer formation, uncontrollable Li dendrite growth, and large volumetric changes of Li metal during the Li stripping and Li plating processes.[8−11] The Li dendrite growth will expose its high surface area to the electrolyte, which accelerates the consumption of the electrolyte and leads to low Coulomb efficiency.[12,13] The uncontrollable Li dendrite formation issue is closely related to the Li plating process, which is affected by the lithiophilic property of the substrate materials.

Considerable efforts have been devoted to addressing the issues of Li dendrite formation. There are several effective strategies, including designing Li alloys with more lithiophobic sites and[7,14−17], creating an artificial SEI layer[18,19], and

Received: April 1, 2022
Accepted: July 1, 2022
Published: July 13, 2022

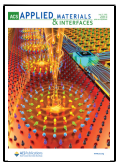

optimizing the electrolyte chemistry.[9,20−24] The lithiophilic sites of the substrate materials are of vital importance for the Li plating process. If the substrate surface maintains numerous lithiophilic sites, Li can adsorb stably and grow smoothly across the substrate surface to produce no Li nucleation overpotential at the beginning of Li plating.[25] The lithiophilic or lithiophobic behavior can be connected with the substrate type. It is reported that the Cu substrate is a lithiophobic material without lithiophilic sites on the surface, which has high Li nucleation energy involved during Li deposition.[25] However, in comparison, the Au substrate is lithiophilic, enabling Li to dissolve into the Au substrate at room temperature to form a Li-alloy buffer layer, which reduces the Li nucleation barrier energy. Besides, Li diffusion on the substrate is another dominant factor for dendrite-free Li plating. Li diffuses faster in Li alloys, such as $Li_{13}In_3$, LiZn, Li_3Bi, and Li_3As, compared to Li metal, where the Li dendrite formation and growth can be suppressed significantly.[14−16,26] The fast Li diffusion can avoid tip effect-induced Li nucleation and thus achieve a uniform Li deposition,[27] whereas a slow Li diffusivity and random Li nucleation process cause a large overpotential. A higher Li diffusion could allow a higher probability for Li to deposit in the vicinity of the substrate instead of being reduced directly on a local protuberant site of the substrate.[28−30] Furthermore, the 3D scaffold structure can adjust the volume change and increase the Li diffusion, resulting in high capacity and good cycling stability.[7,17,31] For example, the innovative 3D Li/$Li_{22}Sn_5$ nanostructure forming a 3D $Li_{22}Sn_5$ interconnected network provides an easy pathway for Li-ion and electron diffusion,[7] which accelerates the Li diffusion and subsequently suppresses the Li dendrite formation and increases the Coulombic efficiency of LMBs.

Although significant efforts have been put into the improvement of the Li plating process from experimental aspects, the fundamental mechanism of the Li deposition process is still unclear. It has been reported that Li diffuses faster on the Li−Sn alloy anode, and it exhibits good cycling stability without dendrite formation.[32] The Li−Sn alloy material can suppress Li dendrite formation effectively and has great potential to be industrialized. Therefore, we focus on the impact of lithiophilic sites of the $Li_{22}Sn_5$ substrate on Li plating. Different from previous works, we concentrate on revealing the fundamental mechanism of the Li plating process on Li metal and $Li_{22}Sn_5$ surface from the atomic and electronic levels and explain why specific Li-alloy materials have better performance compared to Li metal. From a thermodynamic aspect, the adsorption energy is examined to study the Li adsorption process. The reduction energy calculation is conducted to investigate the Li reduction reaction on Li metal and $Li_{22}Sn_5$ surface. From the kinetic aspect, the Li diffusion on $Li_{22}Sn_5$ and Li surfaces is investigated via barrier energy calculation. We found that Li diffusion on the $Li_{22}Sn_5$ surface is a "two Li synergy diffusion" mechanism, while Li diffusion on the Li metal surface is a "single Li diffusion" mechanism. From this, we reveal the physical reasons why Li diffuses faster on the $Li_{22}Sn_5$ surface, resulting in the smooth deposition of Li on the $Li_{22}Sn_5$ surface.

Surface Selection of Li Metal and $Li_{22}Sn_5$. Before studying the impact of lithiophilic sites on the Li plating on Li metal and $Li_{22}Sn_5$ surface, the surface energy is calculated to find the most stable surface facet. The lower surface energy means the surface is more stable. The Li(100), Li(110), Li(111), $Li_{22}Sn_5$(100), $Li_{22}Sn_5$(110), and $Li_{22}Sn_5$(111) surface structures are shown in Figure 1a, which are constructed based on the Li and $Li_{22}Sn_5$ bulk structures. In Figure 1b, we found

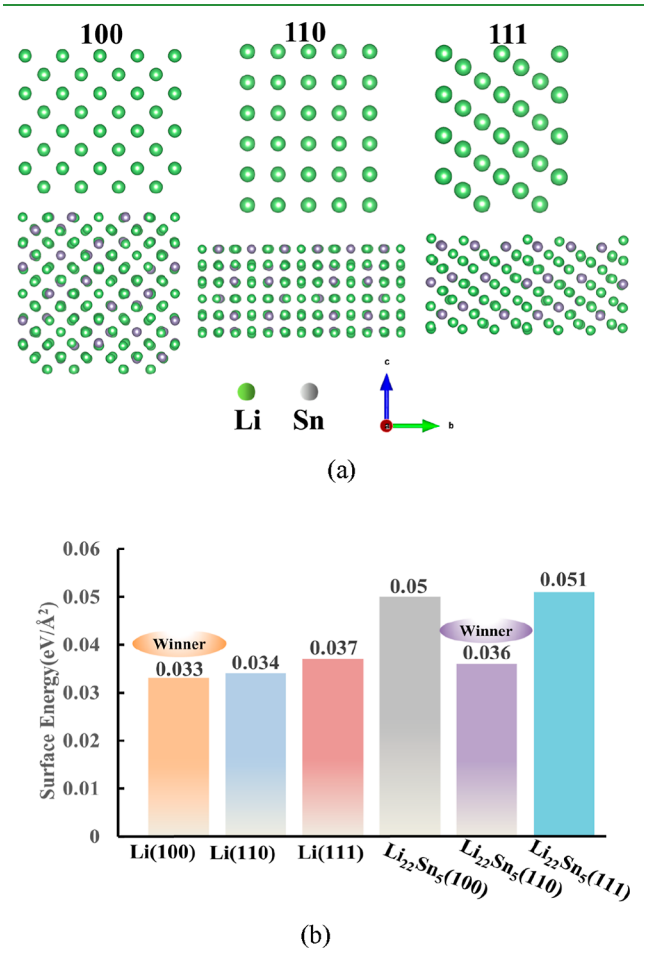

Figure 1. Surface structures (a) and the surface energies (b) of Li(100), Li(110), Li(111), $Li_{22}Sn_5$(100), $Li_{22}Sn_5$(110), and $Li_{22}Sn_5$(111). Li(100) is the most stable surface among Li surface orientations, and $Li_{22}Sn_5$(110) is the most stable surface among $Li_{22}Sn_5$ surface orientations.

that the surface energies of Li(100), Li(110), and Li(111) are 0.033, 0.034, and 0.037 eV/Å^2, respectively, which indicate that the Li(100) surface is the most stable surface. Besides, the surface energies of $Li_{22}Sn_5$(100), $Li_{22}Sn_5$(110), and $Li_{22}Sn_5$(111) are 0.050, 0.036, and 0.051 eV/Å^2 respectively, demonstrating that $Li_{22}Sn_5$(110) is the most stable surface. Therefore, Li(100) and $Li_{22}Sn_5$(110) surfaces are selected for Li adsorption, reduction, and diffusion calculations.

Impact of Lithiophilic Sites on the Li Adsorption Process. The Li adsorption, reduction, and diffusion processes are crucial for Li plating. The Li adsorption process is the first step of Li plating, which is studied by calculating the Li adsorption energy via performing density functional theory (DFT) calculations. The lower Li adsorption energy indicates that Li can be adsorbed on the substrate more easily. The high Li adsorption energy hints that it is difficult for Li to adsorb on the substrate; thus, Li will be desorbed into the electrolyte after being reduced on the substrate, forming Li heterogeneous nucleation in the electrolyte until the Li nucleation cluster size is big enough to drop on the substrate surface. Figure 2a shows one Li adsorbed on Li(100) and $Li_{22}Sn_5$(110) surfaces. Li(100) consists of 128 Li atoms, while $Li_{22}Sn_5$(110) includes

https://doi.org/10.1021/acsami.2c05801
ACS Appl. Mater. Interfaces 2022, 14, 33952−33959

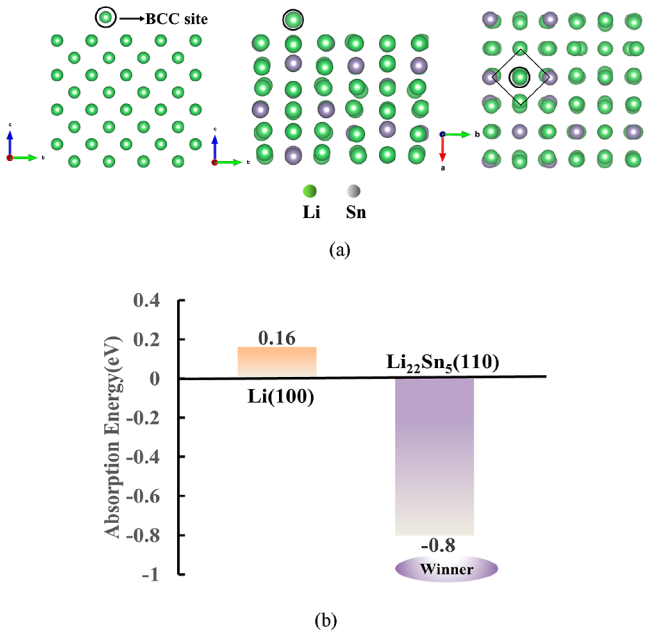

Figure 2. Most stable sites for Li adsorption on Li(100) and $Li_{22}Sn_5$ (110) surfaces (a); Li adsorption energy on Li(100) and $Li_{22}Sn_5$ (110) (b); the Li adsorption energy on $Li_{22}Sn_5$(110) is lower, revealing Li can be adsorbed more stably on the lithiophilic sites of $Li_{22}Sn_5$. However, it is difficult for Li to adsorb tightly on the Li metal surface due to the high adsorption energy, which will desorb into the electrolyte after being reduced on the Li surface.

88 Li and 20 Sn atoms. Several possible Li sites on the Li metal and $Li_{22}Sn_5$ surface are considered, and the Li site with the lowest energy is selected (Figures S1, S2, and Table S1). The Li body-centered cubic (BCC) site on the Li(100) surface shows the lowest adsorption energy, and the Li site on the $Li_{22}Sn_5$(110) surface surrounded by two Sn atoms and three Li atoms has the lowest adsorption energy, as shown in Figure 2a. We found that the Li adsorption energies on Li(100) and $Li_{22}Sn_5$(110) are 0.16 and −0.8 eV, respectively (Figure 2b), indicating that it is easier for Li to be adsorbed on the lithiophilic sites of the $Li_{22}Sn_5$(110) surface than on the Li(100) surface. Therefore, Li adsorbed on the $Li_{22}Sn_5$ surface is stable, while Li cannot stay stably on the Li metal surface due to the high adsorption energy.

Impact of Lithiophilic Sites on the Li Reduction Process. Li reduction on the substrate surface is the second step of the Li plating process. The Li reduction reaction energy on Li metal and $Li_{0.18}/LiSn_{5/22}$ surfaces is calculated. The lower reduction reaction implies that Li can be reduced more easily. The fully relaxed $Li_{0.18}/LiSn_{5/22}$ and Li metal structures with and without Li vacancy are shown in Figure 3a. Figure 3b shows that the Li reduction energies on $Li_{0.18}/LiSn_{5/22}$ and Li are −0.06, and −0.33 eV, respectively, implying that Li can be reduced more easily on the Li metal surface than on the $Li_{0.18}/LiSn_{5/22}$ surface. Besides, the thickness impact of the Li deposition layer is also considered, and it shows that Li can be more easily reduced with the increasing deposition layer of $Li_{1.45}/LiSn_{5/22}$ (Figure S3). As shown in Figure 3c, combining the Li adsorption energy and reduction energy, Li is adsorbed first on the lithiophilic site of $Li_{22}Sn_5$, then reduced to Li metal, and grows on the surface. There is no Li nucleation energy involved during Li deposition on the $Li_{22}Sn_5$ surface. However, Li on the Li metal surface is not stable due to its higher

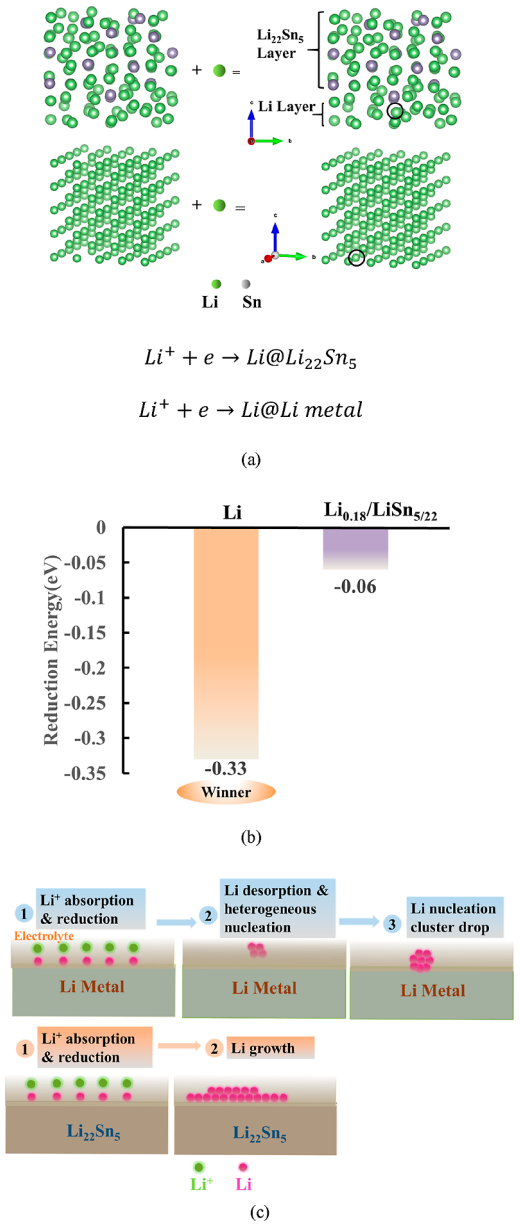

Figure 3. Fully relaxed $Li_{0.18}/LiSn_{5/22}$ and Li metal structures with and without Li^+ vacancy (a); Li reduction energy on the Li metal and $Li_{0.18}/LiSn_{5/22}$ surface (b); Li reduction energy on the Li metal is lower than that on $Li_{0.18}/LiSn_{5/22}$, implying Li can be reduced more easily on the Li metal surface than on the $Li_{0.18}/LiSn_{5/22}$ surface. The lower Li reduction energy on the Li metal surface also indicates that the Fermi energy level of Li is higher than that of $Li_{22}Sn_5$; the schematic of combining the Li adsorption and reduction processes on the Li metal and $Li_{22}Sn_5$ surface (c); Li plating on the $Li_{22}Sn_5$ surface undergoes the "Li adsorption−reduction−growth" process, where there is no extra Li nucleation energy involved. However, Li on the Li metal surface goes through the "Li adsorption−reduction−desorption−heterogenous nucleation−cluster drop" process, causing Li nucleation overpotential during Li plating.

adsorption energy. It desorbs into the electrolyte and forms Li heterogeneous nucleation in the electrolyte. From what has been mentioned above, we can conclude that the lithiophilic sites of the substrate contribute to the dendrite-free Li plating of LMBs.

Voltage Change of $Li_x/LiSn_{5/22}$|Li during Li Plating. To further study the impact of lithiophilic sites of the Li-alloy

https://doi.org/10.1021/acsami.2c05801
ACS Appl. Mater. Interfaces 2022, 14, 33952−33959

substrate on Li plating, the voltage change of $Li_x/LiSn_{5/22}$|Li is calculated during Li deposition on $Li_{22}Sn_5$ paired with Li metal ($0.18 \leq x \leq 1.45$). As we know, there is a relation between voltage and the Fermi level of two electrode materials. A higher voltage indicates a larger Fermi-level difference between Li and $Li_x/LiSn_{5/22}$. Figure 4a shows the $Li_{1.45}LiSn_{5/22}$ and Li metal

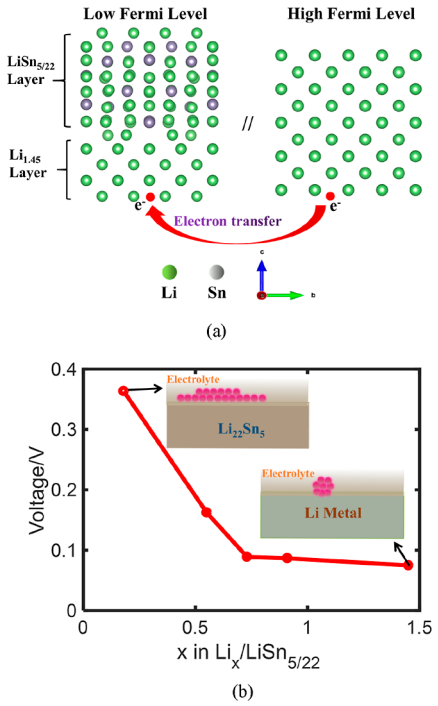

Figure 4. $Li_{1.45}/LiSn_{5/22}$ and Li structures (a); voltage change of $Li_x/LiSn_{5/22}$|Li during Li plating on $Li_{22}Sn_5$ paired with Li metal (b). The voltage of $Li_x/LiSn_{5/22}$|Li decreases from 0.36 to 0.09 V when x increases from 0.18 to 0.73. The voltage of the $Li_x/LiSn_{5/22}$ substrate is almost unchanged when the Li deposition layer further increases. It can be inferred that the Li plating mechanism is the "Li adsorption−reduction−growth" process when Li deposits on the $Li_{22}Sn_5$ surface at the beginning. However, the Li plating mechanism is the "Li adsorption−reduction−desorption−heterogeneous nucleation−cluster drop" process when the Li deposition layer further increases.

structures used for voltage calculation. From Figure 4b, we found that the voltage of $Li_x/LiSn_{5/22}$|Li is more than zero, suggesting that the Fermi energy level of $Li_x/LiSn_{5/22}$ is higher than that of Li metal. Besides, the voltage of $Li_x/LiSn_{5/22}$|Li decreases from 0.36 to 0.09 V when x increases from 0.18 to 0.73 (Table S2), which hints that the Fermi energy difference between $Li_x/LiSn_{5/22}$ and Li metal decreases when the Li deposition layer increases. We also found that the voltage of $Li_x/LiSn_{5/22}$|Li almost stays unchanged after x is more than 0.73. Therefore, we infer that the Li plating mechanism is the "Li adsorption−reduction−growth" process at the beginning of Li deposition on the $Li_{22}Sn_5$ surface. However, the Li deposition mechanism changes to the "Li adsorption−reduction−desorption−heterogeneous nucleation−cluster drop" process when the Li deposition layer further increases.

Impact of Lithiophilic Sites on Li Diffusion Mechanism. Li diffusion on the substrate surface is another important factor for the Li plating of LMBs. A higher Li diffusion means Li is more likely to deposit in the vicinity of the substrate instead of depositing on the protuberant location of the substrate, which helps form a smooth and dense deposition surface.[28−30] The lower barrier energy contributes to a faster Li diffusion on the surface, resulting in a more smooth and uniform deposition on the surface. The Li barrier energy on Li(100) and $Li_{22}Sn_5$(110) is calculated via the CINEB method. The Li diffusion mechanism is closely related to the inherent properties of various transport mediums and external conditions.[33] The Li diffusion in solid materials could be a direct hopping or knock-off mechanism.[34,35] In this work, we focus on the Li diffusion mechanism on the Li metal and $Li_{22}Sn_5$ surface. The direct hopping mechanism is more reasonable in this study, such as a single Li diffusion mechanism, two- or multi-Li synergy diffusion mechanism. The multi-Li synergy diffusion occurs due to the strong interaction between Li and the unique Li configuration in the substrate structure. Thus, the lithiophilic sites on the substrate surface will contribute to faster Li diffusion via two- or multi-Li synergy diffusion mechanisms. In this work, the single Li diffusion and two-Li synergy diffusion mechanisms are identified. There is one type of Li occupation site (BCC site) on the Li metal surface and several types of Li occupation sites on the $Li_{22}Sn_5$ surface during Li diffusion. The results based on the single Li diffusion mechanism show that the barrier energy of Li on Li(100) is 0.042 eV, while the barrier energy of Li on $Li_{22}Sn_5$(110) is 0.286 eV (Figure 5a). The barrier energies based on two-Li diffusion for the Li metal surface and $Li_{22}Sn_5$ surface are 0.178 and 0.035 eV, respectively (Figure 5b), uncovering that Li diffuses faster on the $Li_{22}Sn_5$(110) surface than on the Li(100) surface. To further examine the coordination environment of the Li diffusion on Li(100) and $Li_{22}Sn_5$(110) surfaces, as shown in Figure 5c, we found that the most stable Li site on Li(100) is the bcc site which shows the lowest barrier energy when one Li hops from one bcc site to the nearest site. While the most stable Li site on $Li_{22}Sn_5$ is surrounded by two Sn and three Li, the diffusion barrier energy is the lowest when two combining Li diffuse to the nearest Li sites, and the diffusion pathway of two-Li synergy diffusion on the $Li_{22}Sn_5$(110) surface is shown in Figures S4 and S5. Therefore, as shown in Figure 5d, we disclose that the Li diffusion on the $Li_{22}Sn_5$ surface during Li plating is a "two-Li synergy diffusion" mechanism, while the Li diffusion on the Li metal surface is a "single Li diffusion" mechanism.

CONCLUSIONS

In summary, this work provides a fundamental understanding of the impact of lithiophilic sites on the Li plating mechanism via "Li adsorption", "Li reduction", and "Li diffusion" by performing first-principles calculations. From a thermodynamic aspect, the Li adsorption energy and Li reduction energy are calculated. We found that Li deposition on the lithiophilic $Li_{22}Sn_5$ surface experiences the "Li adsorption−reduction−growth" process. However, the Li deposition on the Li metal surface undergoes the "Li reduction−desorption−heterogeneous nucleation−cluster drop" process. It demonstrates that the Li plating behavior can be regulated by the lithiophilic sites of the $Li_{22}Sn_5$ substrate, uncovering that the lithiophilic sites of the substrate are the dominant factors for nondendrite formation. The lower Li reduction energy on the Li metal surface indicates that Li can be reduced easily on the Li metal surface owing to its higher Fermi energy level. Besides, at the beginning of Li deposition on the $Li_{22}Sn_5$ surface, the Li plating mechanism is the "Li adsorption−reduction−growth" process. However, it changes to the "Li adsorption−

https://doi.org/10.1021/acsami.2c05801
ACS Appl. Mater. Interfaces 2022, 14, 33952−33959

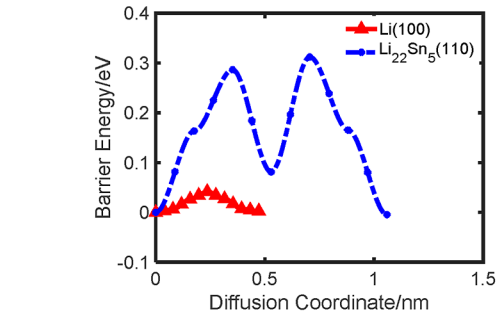

(a)

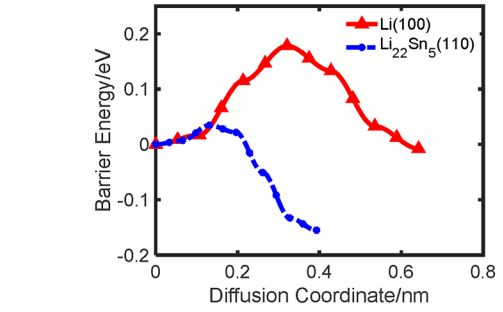

(b)

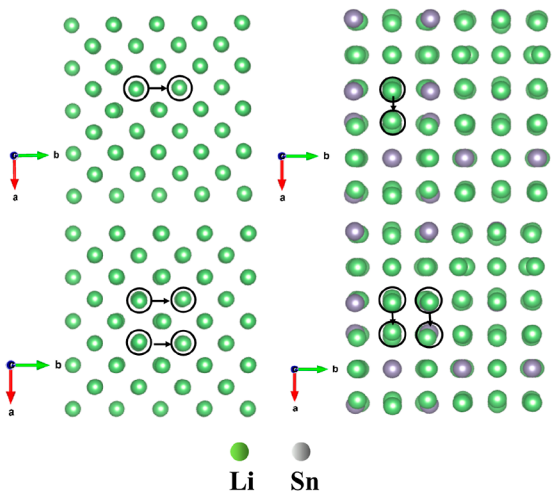

(c)

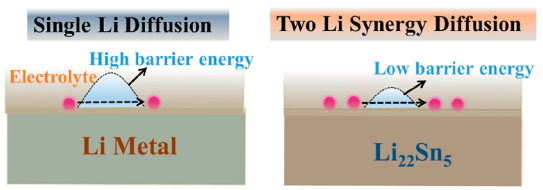

(d)

Figure 5. One- (a) and two- (b) Li diffusion on Li(100) and $Li_{22}Sn_5$(110) surfaces; initial Li and final Li sites of single Li diffusion and two-Li synergy diffusion on the Li(100) and $Li_{22}Sn_5$(110) surfaces (c); the schematic of the Li diffusion mechanism on the Li metal and $Li_{22}Sn_5$ surface (d). It demonstrates that Li diffuses faster on $Li_{22}Sn_5$ than on the Li metal surface. The Li diffusion on the $Li_{22}Sn_5$ metal surface is a "two-Li synergy diffusion" mechanism, and the Li diffusion on the Li metal surface is a "single Li diffusion" mechanism.

reduction−desorption−heterogeneous nucleation−cluster drop" process when the Li deposition layer increases. From the kinetic aspect, we found that the Li diffusion behavior can be adjusted by the lithiophilic sites of $Li_{22}Sn_5$, and Li diffuses faster on the $Li_{22}Sn_5$ surface due to its lower barrier energy. We disclose that Li diffusion on the $Li_{22}Sn_5$ surface is a "two-Li synergy diffusion" mechanism, while Li diffusion on the Li metal surface is a "single Li diffusion" mechanism. This work reveals the fundamental Li adsorption, Li reduction, and Li diffusion mechanisms on the Li-alloy surface from the atomic and electronic aspects, which gives a new insight into the impact of lithiophilic sites on the Li plating process and explains why there exists Li nucleation overpotential during Li plating. It guides the future design of 3D Li-alloy substrates decorated with multilithiophilic sites that can prevent dendrite formation on the lithium-alloy substrate by guiding uniform Li deposition.

COMPUTATIONAL METHOD

The first-principles calculation is performed by using Vienna Ab-initio Simulation Package code.[36] The Perdew−Burke−Ernzerhof functional is applied to approximate the exchange−correlation functional, and the projector augmented-wave method[37−39] is used for electron and core interaction. The projection operators are evaluated in real space. The cutoff energy is set to be 400 eV. The vacuum thickness is 15 Å for all slab structures to prevent the interaction between the periodic images. All calculations reach the required energy convergence. The accuracy for electronic minimization is 10^{-4} eV, and the stopping criterion for ionic relaxation is 0.03 eV/Å. During the Li adsorption, Li reduction, and Li diffusion calculations, the van der Waals interaction is considered by using the DFT-D3 method with Becke−Jonson damping,[40] and the dipole corrections are applied in the z direction to counterbalance the size effect of the supercell due to the periodic boundary conditions. The surface energies of different surface orientations of Li and $Li_{22}Sn_5$ are verified to find the most stable surface. The low-index 100, 110, and 111 surfaces of Li and $Li_{22}Sn_5$ are considered during surface energy calculations. The $Li_{22}Sn_5$ surfaces are created via Materials Studio based on the bulk structure from the Ceder group [mp-1198729: $Li_{22}Sn_5$ (cubic, $F\bar{4}3m$, 216)].[41] To guarantee the accuracy of the surface energy calculation for $Li_{22}Sn_5$, the slab sizes of $Li_{22}Sn_5$ (100), (110), and (111) are 19.73 Å × 19.73 Å, 19.73 Å × 27.90 Å, 27.90 Å × 27.90 Å, respectively. The surface energy σ defines the energy difference between a newly generated surface and that of the bulk structure[42]

$$\sigma = (E_{slab} - E_{bulk})/2A \quad (1)$$

where E_{slab} is the total energy of the slab structure, E_{bulk} is the total energy of the bulk structure, and A is the area surface.

After obtaining the most stable Li and $Li_{22}Sn_5$ surfaces, the Li adsorption behavior on the Li metal and $Li_{22}Sn_5$ surface is investigated. The slab size of $Li_{22}Sn_5$(110) decreases to 13.95 Å × 13.95 Å to reduce the computational resource. The Li(100) slab structure consists of eight layers, and the $Li_{22}Sn_5$(110) slab structure includes six layers. The Li(100) structure is fully relaxed by fixing the bottom four layers, and $Li_{22}Sn_5$(110) is fully optimized by fixing the bottom three layers. Several possible adsorption sites are considered, and the most stable site is selected for adsorption energy calculation on the Li(100) and $Li_{22}Sn_5$(110) surfaces. The Li adsorption energy E_{adsorb} is described as follows[43]

https://doi.org/10.1021/acsami.2c05801
ACS Appl. Mater. Interfaces 2022, 14, 33952−33959

$$E_{adsorb} = E_{slab+Li} - (E_{slab} + E_{Li}) \quad (2)$$

where $E_{slab+Li}$ is the total energy of the slab structure with one Li adsorbed on the surface, E_{slab} is the total energy of the surface structure, and E_{Li} is the total energy of one Li.

The Li reduction energy is calculated to investigate the Li reduction process during Li plating. The Li reduction energy is the energy needed for Li to be reduced on the Li metal or $Li_{0.18}/LiSn_{5/22}$ surface. The $Li_{0.18}/LiSn_{5/22}$ structure is a $LiSn_{5/22}$ slab with one deposited Li layer. Several reduction sites for Li on the Li metal and $Li_x/LiSn_{5/22}$ are considered, and the reduction site with the lowest energy is selected for Li reduction energy calculation. The Li reduction energy $E_{reduction}$ can be expressed as follows[42,44]

$$E_{reduction} = E_{slab} - (E_{with\ Li^+\ vacancy} + E_{Li^+}) \quad (3)$$

where E_{slab} is the total energy of the Li metal or $Li_x/LiSn_{5/22}$ structure, $E_{with\ Li^+\ vacancy}$ is the total energy of the Li metal or $Li_{x-1}/LiSn_{5/22}$ structure with one Li^+ vacancy and one extra electron, and E_{Li^+} is the total energy of one Li^+.

Besides, the voltage of $Li_x/LiSn_{5/22}$|Li is calculated ($0.18 \leq x \leq 1.45$) to study the voltage variation of $Li_x/LiSn_{5/22}$|Li during the Li plating process. It compares the Fermi energy level of $Li_x/LiSn_{5/22}$ and Li metal during Li plating. The voltage of the $Li_x/LiSn_{5/22}$|Li formula is expressed as follows[45,46]

$$V = [E_{Li_{x+dx}/LiSn_{5/22}} - E_{Li_x/LiSn_{5/22}}] + E_{Li} \quad (4)$$

where $E_{Li_{x+dx}/LiSn_{5/22}}$ and $E_{Li_x/LiSn_{5/22}}$ stand for the total energy before and after dx Li extraction from the $Li_{x+dx}/LiSn_{5/22}$ compound per formula unit, respectively, while E_{Li} is the total energy of the Li metal.

The Li diffusion mechanism is also investigated via the climbing image-nudged elastic band (CINEB)[47] method. The barrier energy of Li diffusion can be obtained via CINEB calculation, and the low barrier energy indicates that Li diffuses faster from the initial site to the final site. For one- and two-Li diffusion calculations on the Li metal and $Li_{22}Sn_5$ surface, the energies of several initial and final configurations are tested, and the configurations with the lowest energies are selected for CINEB calculations. Several diffusion paths have been examined, and the diffusion pathway with the lowest diffusion barrier energy is chosen. During CINEB calculations, five images are inserted between the initial and final states during optimization. The criteria for ionic relaxation and electronic self-consistency are set to be 10^{-4} eV and 0.03 eV/Å, respectively.

ASSOCIATED CONTENT

Supporting Information

The Supporting Information is available free of charge at https://pubs.acs.org/doi/10.1021/acsami.2c05801.

> Li adsorption energy on Li(100), $Li_{22}Sn_5$(110), and $Li_{22}Sn_5$(100) surfaces; different possible adsorption sites on the Li(100) and $Li_{22}Sn_5$ (110) surfaces; Li reduction energies on Li, $Li_{0.18}/LiSn_{5/22}$, and $Li_{1.45}/LiSn_{5/22}$; diffusion pathway of two-Li synergy diffusion on the $Li_{22}Sn_5$(110) surface (PDF)

AUTHOR INFORMATION

Corresponding Authors

Li Wang − *Institute of Nuclear and New Energy Technology, Tsinghua University, Beijing 100084, China;* orcid.org/0000-0002-9615-1879; Email: wang-l@tsinghua.edu.cn

Jonghyun Park − *Department of Mechanical Engineering and Aerospace Engineering, Missouri University of Science and Technology, Rolla, Missouri 65401, United States;* orcid.org/0000-0003-4241-3842; Email: parkjonghy@mst.edu

Xiangming He − *Institute of Nuclear and New Energy Technology, Tsinghua University, Beijing 100084, China;* orcid.org/0000-0001-7146-4097; Email: hexm@tsinghua.edu.cn

Authors

Yufang He − *Institute of Nuclear and New Energy Technology, Tsinghua University, Beijing 100084, China*

Mengyun Zhang − *Institute of Nuclear and New Energy Technology, Tsinghua University, Beijing 100084, China*

Aiping Wang − *Institute of Nuclear and New Energy Technology, Tsinghua University, Beijing 100084, China*

Bo Zhang − *Institute of Nuclear and New Energy Technology, Tsinghua University, Beijing 100084, China*

Hiep Pham − *Department of Mechanical Engineering and Aerospace Engineering, Missouri University of Science and Technology, Rolla, Missouri 65401, United States*

Qiao Hu − *Institute of Nuclear and New Energy Technology, Tsinghua University, Beijing 100084, China*

Li Sheng − *Institute of Nuclear and New Energy Technology, Tsinghua University, Beijing 100084, China*

Hong Xu − *Institute of Nuclear and New Energy Technology, Tsinghua University, Beijing 100084, China;* orcid.org/0000-0001-7918-1454

Complete contact information is available at: https://pubs.acs.org/10.1021/acsami.2c05801

Author Contributions

Y.H. performed theoretical simulations and wrote the draft of the manuscript; X.H. and L.W. provided guidance and ideas for this work; J.P. and H.P. modified the manuscript; M.Z. contributed to plotting figures; A.W., B.Z., Q.H., L.S., and H.X. provided meaningful suggestions for the manuscript and calculations.

Notes

The authors declare no competing financial interest.

ACKNOWLEDGMENTS

This work was supported by the National Natural Science Foundation of China (no. U21A20170), the Ministry of Science and Technology of China (no. 2019YFA0705703), and China Postdoctoral Science Foundation [no. 2021M701873 (B.Z.), 2022M711791 (Y.H.)]. The authors also thank Joint Work Plan for Research Projects under the Clean Vehicles Consortium at U.S. and China—Clean Energy Research Center (CERC-CVC) and the Tsinghua University−Zhangjiagang Joint Institute for Hydrogen Energy and Lithium-Ion Battery Technology.

REFERENCES

(1) Armand, M.; Tarascon, J.-M. Building better batteries. *Nature* **2008**, *451*, 652−657.

(2) Manthiram, A. An Outlook on Lithium Ion Battery Technology. *ACS Cent. Sci.* **2017**, *3*, 1063−1069.
(3) Goodenough, J. B.; Park, K.-S. The Li-ion rechargeable battery: a perspective. *J. Am. Chem. Soc.* **2013**, *135*, 1167−1176.
(4) Wang, S.-H.; Yin, Y.-X.; Zuo, T.-T.; Dong, W.; Li, J.-Y.; Shi, J.-L.; Zhang, C.-H.; Li, N.-W.; Li, C.-J.; Guo, Y.-G. Stable Li Metal Anodes via Regulating Lithium Plating/Stripping in Vertically Aligned Microchannels. *Adv. Mater.* **2017**, *29*, 1703729.
(5) Sun, Y.; Liu, N.; Cui, Y. Promises and challenges of nanomaterials for lithium-based rechargeable batteries. *Nat. Energy* **2016**, *1*, 16071.
(6) Xu, W.; Wang, J.; Ding, F.; Chen, X.; Nasybulin, E.; Zhang, Y.; Zhang, J.-G. Lithium metal anodes for rechargeable batteries. *Energy Environ. Sci.* **2014**, *7*, 513−537.
(7) Wan, M.; Kang, S.; Wang, L.; Lee, H.-W.; Zheng, G. W.; Cui, Y.; Sun, Y. Mechanical rolling formation of interpenetrated lithium metal/lithium tin alloy foil for ultrahigh-rate battery anode. *Nat. Commun.* **2020**, *11*, 829.
(8) Liu, B.; Zhang, J.-G.; Xu, W. Advancing Lithium Metal Batteries. *Joule* **2018**, *2*, 833−845.
(9) Lu, Y.; Tu, Z.; Archer, L. A. Stable lithium electrodeposition in liquid and nanoporous solid electrolytes. *Nat. Mater.* **2014**, *13*, 961−969.
(10) Cao, R.; Xu, W.; Lv, D.; Xiao, J.; Zhang, J.-G. Anodes for Rechargeable Lithium-Sulfur Batteries. *Adv. Energy Mater.* **2015**, *5*, 1402273.
(11) Li, N.-W.; Shi, Y.; Yin, Y.-X.; Zeng, X.-X.; Li, J.-Y.; Li, C.-J.; Wan, L.-J.; Wen, R.; Guo, Y.-G. A Flexible Solid Electrolyte Interphase Layer for Long-Life Lithium Metal Anodes. *Angew. Chem., Int. Ed.* **2018**, *57*, 1505−1509.
(12) Sheng, L.; Wu, Y.; Tian, J.; Wang, L.; Wang, J.; Tang, Y.; Xu, H.; He, X. Impact of lithium-ion coordination on lithium electrodeposition. *Energy Environ. Mater.* **2021**, *5*, 386.
(13) Liu, J.; Bao, Z.; Cui, Y.; Dufek, E. J.; Goodenough, J. B.; Khalifah, P.; Li, Q.; Liaw, B. Y.; Liu, P.; Manthiram, A.; Meng, Y. S.; Subramanian, V. R.; Toney, M. F.; Viswanathan, V. V.; Whittingham, M. S.; Xiao, J.; Xu, W.; Yang, J.; Yang, X.-Q.; Zhang, J.-G. Pathways for practical high-energy long-cycling lithium metal batteries. *Nat. Energy* **2019**, *4*, 180−186.
(14) Hiratani, M.; Miyauchi, K.; Kudo, T. Effect of a lithium alloy layer inserted between a lithium anode and a solid electrolyte. *Solid State Ionics* **1988**, *28*−*30*, 1406−1410.
(15) Liang, X.; Pang, Q.; Kochetkov, I. R.; Sempere, M. S.; Huang, H.; Sun, X.; Nazar, L. F. A facile surface chemistry route to a stabilized lithium metal anode. *Nat. Energy* **2017**, *2*, 17119.
(16) Shi, Z. Electrochemical Properties of Li-Zn Alloy Electrodes Prepared by Kinetically Controlled Vapor Deposition for Lithium Batteries. *Electrochem. Solid-State Lett.* **1999**, *3*, 312.
(17) Shimizu, M.; Munkhbat, M.; Arai, S. Li-insertion/extraction properties of three-dimensional Sn electrode prepared by facile electrodeposition method. *J. Appl. Electrochem.* **2017**, *47*, 727−734.
(18) Li, N.-W.; Yin, Y.-X.; Yang, C.-P.; Guo, Y.-G. An Artificial Solid Electrolyte Interphase Layer for Stable Lithium Metal Anodes. *Adv. Mater.* **2016**, *28*, 1853−1858.
(19) Xu, R.; Liu, F.; Ye, Y.; Chen, H.; Yang, R. R.; Ma, Y.; Huang, W.; Wan, J.; Cui, Y. A Morphologically Stable Li/Electrolyte Interface for All-Solid-State Batteries Enabled by 3D-Micropatterned Garnet. *Adv. Mater.* **2021**, *33*, 2104009.
(20) Piao, N.; Liu, S.; Zhang, B.; Ji, X.; Fan, X.; Wang, L.; Wang, P.-F.; Jin, T.; Liou, S.-C.; Yang, H.; Jiang, J.; Xu, K.; Schroeder, M. A.; He, X.; Wang, C. Lithium Metal Batteries Enabled by Synergetic Additives in Commercial Carbonate Electrolytes. *ACS Energy Lett.* **2021**, *6*, 1839−1848.
(21) Shangguan, X.; Xu, G.; Cui, Z.; Wang, Q.; Du, X.; Chen, K.; Huang, S.; Jia, G.; Li, F.; Wang, X.; Lu, D.; Dong, S.; Cui, G. Additive-Assisted Novel Dual-Salt Electrolyte Addresses Wide Temperature Operation of Lithium−Metal Batteries. *Small* **2019**, *15*, 1900269.
(22) Wu, L.-N.; Peng, J.; Han, F.-M.; Sun, Y.-K.; Sheng, T.; Li, Y.-Y.; Zhou, Y.; Huang, L.; Li, J.-T.; Sun, S.-G. Suppressing lithium dendrite growth by a synergetic effect of uniform nucleation and inhibition. *J. Mater. Chem. A* **2020**, *8*, 4300−4307.
(23) Ren, X.; Zhang, Y.; Engelhard, M. H.; Li, Q.; Zhang, J.-G.; Xu, W. Guided Lithium Metal Deposition and Improved Lithium Coulombic Efficiency through Synergistic Effects of LiAsF6 and Cyclic Carbonate Additives. *ACS Energy Lett.* **2018**, *3*, 14−19.
(24) Shi, P.; Liu, F.; Feng, Y.; Zhou, J.; Rui, X.; Yu, Y. The Synergetic Effect of Lithium Bisoxalatodifluorophosphate and Fluoroethylene Carbonate on Dendrite Suppression for Fast Charging Lithium Metal Batteries. *Small* **2020**, *16*, No. e2001989.
(25) Yan, K.; Lu, Z.; Lee, H.-W.; Xiong, F.; Hsu, P.-C.; Li, Y.; Zhao, J.; Chu, S.; Cui, Y. Selective deposition and stable encapsulation of lithium through heterogeneous seeded growth. *Nat. Energy* **2016**, *1*, 16010.
(26) Wang, J.; Hu, H.; Duan, S.; Xiao, Q.; Zhang, J.; Liu, H.; Kang, Q.; Jia, L.; Yang, J.; Xu, W.; Fei, H.; Cheng, S.; Li, L.; Liu, M.; Lin, H.; Zhang, Y. Construction of Moisture-Stable Lithium Diffusion-Controlling Layer toward High Performance Dendrite-Free Lithium Anode. *Adv. Funct. Mater.* **2021**, *32*, 2110468.
(27) Zhou, S.; Chen, W.; Shi, J.; Li, G.; Pei, F.; Liu, S.; Ye, W.; Xiao, L.; Wang, M.-S.; Wang, D.; Qiao, Y.; Huang, L.; Xu, G.-L.; Liao, H.-G.; Chen, J.-F.; Amine, K.; Sun, S.-G. Efficient diffusion of superdense lithium via atomic channels for dendrite-free lithium−metal batteries. *Energy Environ. Sci.* **2022**, *15*, 196.
(28) Mayers, M. Z.; Kaminski, J. W.; Miller, T. F. Suppression of Dendrite Formation via Pulse Charging in Rechargeable Lithium Metal Batteries. *J. Phys. Chem. C* **2012**, *116*, 26214−26221.
(29) Li, L.-x.; Tang, X.-c.; Qu, Y.; Liu, H.-t. CC-CV charge protocol based on spherical diffusion model. *J. Cent. S. Univ.* **2011**, *18*, 319−322.
(30) Li, Z.; Huang, J.; Yann Liaw, B.; Metzler, V.; Zhang, J. A review of lithium deposition in lithium-ion and lithium metal secondary batteries. *J. Power Sources* **2014**, *254*, 168−182.
(31) Okamoto, N.; Morita, K.; Saito, T. Sn Negative Electrode Consists of Flexible 3D Structures for Sodium Ion Secondary Batteries. *ECS Trans.* **2017**, *75*, 59−66.
(32) Tu, Z.; Choudhury, S.; Zachman, M. J.; Wei, S.; Zhang, K.; Kourkoutis, L. F.; Archer, L. A. Fast ion transport at solid−solid interfaces in hybrid battery anodes. *Nat. Energy* **2018**, *3*, 310−316.
(33) Ren, Y.; Zhe-Yi, Z.; Qian, Z.; Da, W.; Jia, Y.; Si-Qi, S. Brief overview of microscopic physical image of ion transport in electrolytes. *Acta Phys. Sin.* **2020**, *69*, 226601.
(34) He, X.; Zhu, Y.; Mo, Y. Origin of fast ion diffusion in superionic conductors. *Nat. Commun.* **2017**, *8*, 15893.
(35) Shi, S.; Lu, P.; Liu, Z.; Qi, Y.; Hector, L. G., Jr.; Li, H.; Harris, S. J. Direct calculation of Li-ion transport in the solid electrolyte interphase. *J. Am. Chem. Soc.* **2012**, *134*, 15476−15487.
(36) Hafner, J.; Kresse, G. The Vienna AB-Initio Simulation Program VASP: An Efficient and Versatile Tool for Studying the Structural, Dynamic, and Electronic Properties of Materials. In *Properties of Complex Inorganic Solids*; Gonis, A., Meike, A., Turchi, P. E. A., Eds.; Springer US: Boston, MA, 1997; pp 69−82.
(37) Perdew, J. P.; Burke, K.; Ernzerhof, M. Generalized Gradient Approximation Made Simple. *Phys. Rev. Lett.* **1996**, *77*, 3865−3868.
(38) Kresse, G.; Furthmüller, J. Efficient iterative schemes for ab initio total-energy calculations using a plane-wave basis set. *Phys. Rev. B: Condens. Matter Mater. Phys.* **1996**, *54*, 11169−11186.
(39) Kresse, G.; Furthmüller, J. Efficiency of ab-initio total energy calculations for metals and semiconductors using a plane-wave basis set. *Comput. Mater. Sci.* **1996**, *6*, 15−50.
(40) Grimme, S.; Ehrlich, S.; Goerigk, L. Effect of the damping function in dispersion corrected density functional theory. *J. Comput. Chem.* **2011**, *32*, 1456−1465.
(41) Gladyshevskii, E. I.; Kripyakevich, P. I. New examples of the structural type $Li_{22}Pb_5$. *Sov. Phys. Crystallogr.* **1964**, *9*, 338−341.
(42) He, Y.; Pham, H.; Gao, Y.; Patel, R. L.; Sarkar, S.; Liang, X.; Park, J. Discovery of an Unexpected Metal Dissolution of Thin-Coated Cathode Particles and Its Theoretical Explanation. *Adv. Theory Simul.* **2020**, *3*, 2000002.

(43) Li, S.; Fu, J.; Miao, G.; Wang, S.; Zhao, W.; Wu, Z.; Zhang, Y.; Yang, X. Toward Planar and Dendrite-Free Zn Electrodepositions by Regulating Sn-Crystal Textured Surface. *Adv. Mater.* **2021**, *33*, 2008424.
(44) Tompsett, D. A.; Parker, S. C.; Islam, M. S. Rutile (β-)MnO_2 surfaces and vacancy formation for high electrochemical and catalytic performance. *J. Am. Chem. Soc.* **2014**, *136*, 1418−1426.
(45) Yu, H.; Qian, Y.; Otani, M.; Tang, D.; Guo, S.; Zhu, Y.; Zhou, H. Study of the lithium/nickel ions exchange in the layered $LiNi_{0.42}Mn_{0.42}Co_{0.16}O_2$ cathode material for lithium ion batteries: experimental and first-principles calculations. *Energy Environ. Sci.* **2014**, *7*, 1068−1078.
(46) Wang, H.; Jing, Z.; Liu, H.; Feng, X.; Meng, G.; Wu, K.; Cheng, Y.; Xiao, B. A high-throughput assessment of the adsorption capacity and Li-ion diffusion dynamics in Mo-based ordered double-transition-metal MXenes as anode materials for fast-charging LIBs. *Nanoscale* **2020**, *12*, 24510−24526.
(47) Caspersen, K. J.; Carter, E. A. Finding transition states for crystalline solid-solid phase transformations. *Proc. Natl. Acad. Sci. U.S.A.* **2005**, *102*, 6738−6743.

https://doi.org/10.1021/acsami.2c05801
ACS Appl. Mater. Interfaces 2022, 14, 33952−33959